# The Kondo Problem and the Numerical Renormalization Group

Term Project

PHYS4240: Solid State Physics

Casey Hampson

May 3, 2025

# Contents

# 1 Introduction

In the early 1930s, experiments revealed contradictions in the resistance of certain metals in the low energy regime [1]. In particular, the expectation at the time was that the resistance should monotonically decrease, since it is directly related to electron-phonon interactions/scattering, which decrease with decreasing temperature. However, it was found that this is not the case; in fact, the resistance of these metals reached a minimum at some temperature and then started increasing again (see Fig. 1.1 for this behavior in gold). It eventually became clear that this was due to magnetic impurities in these particular metals.

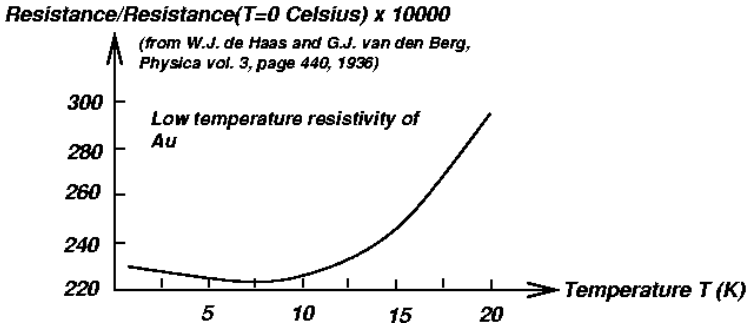


Figure 1.1: Figure created using the resistivity measurements found in Ref. [2].

At this point, a number of models were introduced in an attempt to describe a system with metallic impurities, a couple of which being the Anderson model and the s-d exchange model. These were very simple models and only account for some of the behavior observed in experiment. In 1964, one major breakthrough occurred when Jun Kondo formulated the problem as a model in which the spin of the conduction electrons interacted with that of the magnetic impurity.[1] The Hamiltonian he formulated for this system looks like:

$$\hat{H} = \sum_{\mathbf{k},\sigma} \epsilon_{\mathbf{k}} c^{\dagger}_{\mathbf{k},\sigma} c_{\mathbf{k},\sigma} + J \sum_{\mathbf{k},\mathbf{k}',\alpha,\beta} c^{\dagger}_{\mathbf{k},\alpha} \boldsymbol{\sigma}_{\alpha,\beta} c_{\mathbf{k}',\beta} \cdot \mathbf{S}, \tag{1.1}$$

where $c^{\dagger}_{\mathbf{k},\sigma}$ and $c_{\mathbf{k},\sigma}$ are the creation and annihilation operators for Bloch states representing the conduction electrons with a wavevector $\mathbf{k}$ and spin $\sigma$, $\epsilon_{\mathbf{k}}$ is the energy eigenvalue, $\mathbf{S}$ is the spin of the impurity, and $J$ is the coupling strength. Kondo then applied perturbation theory with this spin-spin interaction as the perturbation up to third order and retrieved results [3] which matched quite well with experiment; a functional form for the resistance goes like:

$$R(T) = aT^5 + c_{\text{imp}} R_0 - c_{\text{imp}} R_1 \ln\left(\frac{k_B T}{D}\right), \tag{1.2}$$

with the first term coming from the expected electron-phonon interactions and the second and third terms coming from perturbation theory related to the impurity. The logarithmic term did indeed successfully account for the resistance minimum and subsequent increasing as temperature decreased, but obviously, at a certain point it diverges. The point at which this singular behavior starts dominating is called the *Kondo temperature* $T_K$, given roughly by

$$k_B T_K \approx D \exp\left[-\frac{1}{2J\rho}\right], \tag{1.3}$$

with $D$ being the band width for the conduction electrons and $\rho$ being the density of states.

Evidently, despite accurately providing results in a particular low temperature regime, Kondo's solution wasn't perfect, and a better model was required in order to explain impurities in metals for temperatures at and below the Kondo temperature. This issue was henceforth dubbed "The Kondo Problem".

[1] He didn't declare *where* the spin moment came from, only that it was there; Anderson's model, as we will see, attempts to explain where it comes from.

## 1.1 Subsequent Notable Breakthroughs

Soon afterwards, Philip Anderson introduced what was effectively a modifed renormalization scheme dubbed "poor man's scaling" [4]. The essential recipe was a continuous scaling of the cutoff energy along with integrating out higher energy effects such that only the lower energy contributions remained, yielding an effective Hamiltonian valid at a lower energy. The effective Hamiltontian it yielded was of the same form as the previously unscaled one; the assumption that this same form would hold for the new system was an assumption, but turned out to work well. The reason for its name was that Anderson's scaling method wasn't quite how traditional renormalization schemes were typically conducted.

Unfortunately, so too did Anderson's scaling approach fail in the very low temperature regime. The reason for this was that upon successive scalings of the energy, the coupling strength between the impurity and the conduction electrons increased without bound – it was *renormalized*. This was an issue because the scaling method was in part possible due to a perturbative expansion about this coupling. Once this parameter was no longer small, the perturbative scheme no longer worked. This, again, yielded a non-zero temperature below which results were not accurate.

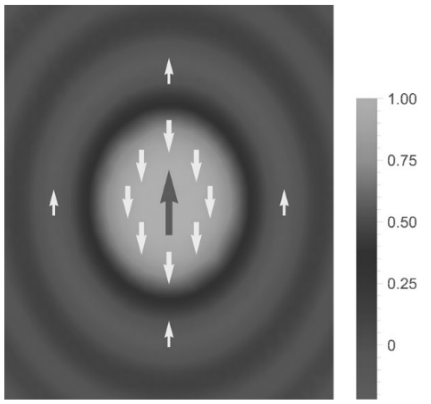


Figure 1.2: The Kondo cloud, representing the induced spin density due to the bound state of the impurity and conduction electron bound state.

However, despite this method not yielding results all the way to $T = 0$, its qualitative results were very significant. The fact that the coupling increased without bound indicated that the impurity and the conduction electrons formed a bound state. Other conduction electrons then screen this bound state, leading to an induced spin density that many like to call the Kondo cloud (see Fig. 1.2). Crudely summarizing, at higher energies the typical electron-phonon interactions dominate since they go like $T^5$. Then, they reach a minimum, after which the increasing coupling between the impurity and the conduction electrons form a singlet and induce a spin density that screens the singlet, which, roughly speaking, increases the resistance as the bound state forms a scattering center.

Kenneth Wilson eventually took inspriation from this approach and utilized a method derived from the numerical renormalization group (NRG) [5], which did not involve perturbative expansion about a coupling that grew without bound, but rather about a generic small parameter $\Lambda$ related to the energy scaling factor, which remained small through the renormalization procedure. Because of this, Wilson's method was accurate at all energy scales, and finally produced coherent results for many properties at these energy scales, as well as confirming the qualitative result reached by Anderson and understanding how it is interpreted in NRG language.

As a connection to high-energy physics, this concept of a coupling increasing without bound is sort of a inverse *asymptotic freedom* that we observe with quarks. In the latter case, the strong force (the coupling between the quarks) *decreases* to zero at higher energies. At sufficient energies, our perturbative formalism becomes better and better. Consequently, this means the coupling *increases* at *lower* energies, meaning our perturbative formalism becomes inadequate. Methods like lattice QCD are being studied which have been effective so far at generating results at energies in which the coupling is too large to apply perturbation theory.

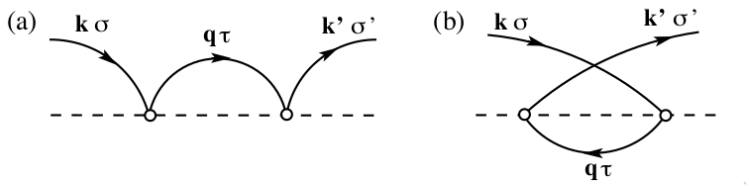


Figure 2.1: Feynman diagrams describing the spin scattering of the impurity electron and conduction electron used to calculate the $T$-matrix elements.

# 2 Poor Man's Scaling

We first quote some results from Anderson's scaling method, as it is instructive to see where the qualitative conclusion of increasing coupling comes from, as well as why its successive renormalization means it fails in the low temperature regime.

## 2.1 The Scattering $T$-Matrix

The way this was calculated was via the scattering $T$-matrix. This is very similar to the born series, which looks like

$$\psi = \psi_0 + \int gV\psi_0 + \int\int gVgV\psi_0 + \int\int\int gVgVgV\psi_0 + \dots. \tag{2.1}$$

This is a way to achieve approximate scattering results via a Green's function $g$ and a potential $V$. The $T$-matrix representing scattering of an electron from an initial state $|\mathbf{k}\rangle$ to final state $|\mathbf{k}'\rangle$ looks like, to second order:

$$T_{\mathbf{k},\mathbf{k}}(\omega) = V_{\mathbf{k}',\mathbf{k}} + V_{\mathbf{k}',\mathbf{q}}G_0(\omega,\mathbf{q})T(\omega). \tag{2.2}$$

Feynman diagrams for this process are given in Fig. 2.1. Here, the "potential" term $V$ is related to the coupling; hence, to second order, what we have upon doing this calculation is the effective renormalization of the potential, which corresponds to the coupling $J$:

$$\hat{V} \to \hat{V}' = \hat{V} + \hat{V}\frac{1}{\omega - \hat{H}_0}\hat{V}, \tag{2.3}$$

where

$$G_0 = \frac{1}{\omega - \hat{H}_0} \tag{2.4}$$

is the Green's function. At this point, I will now quote results, as it would have been far too challenging to exhaustively study this as well as the NRG. As Eq. (2.3) implies, we have a normalization of the coupling like $J_\alpha \to J_\alpha + \delta J_\alpha$, where $\alpha = \pm, z$. Anderson found that the forms of the $\delta J_\alpha$s look like:

$$\delta J_z = -J_\pm^2\rho|\delta\Lambda|\left[\frac{1}{\omega - \Lambda + \epsilon_k} + \frac{1}{\omega - \Lambda - \epsilon_{k'}}\right], \tag{2.5}$$

$$\delta J_\pm = -J_z J_\pm\rho|\delta\Lambda|\left[\frac{1}{\omega - \Lambda + \epsilon_k} + \frac{1}{\omega - \Lambda - \epsilon_{k'}}\right]. \tag{2.6}$$

Introducing dimensionless coupling constants $g_\alpha \equiv \rho J_\alpha$, we are able to find renormalization flow equations that look like:

$$\frac{\mathrm{d}g_z}{\mathrm{d}\ln\Lambda} = -2g_\pm^2 + \mathcal{O}(g^3), \tag{2.7}$$

$$\frac{\mathrm{d}g_\pm}{\mathrm{d}\ln\Lambda} = -2g_z g_\pm + \mathcal{O}(g^3). \tag{2.8}$$

### 2.2 Qualitative Conclusions

There is one important case to consider: the antiferromagnetic one. In this case, the couplings are positive, so the overall minus remains. This signifies that as the energy decreases, the coupling will increase without bound. This was one main result from this method; however, the other was that the $T$-matrix formalism, i.e. expansion up to second order, is valid insofar as the coupling (represented by $V$) remains small. However, it clearly shoots up to infinity, making this method incompatible with the very low-energy regime.

Despite this failure, the increasing coupling was not disregarded. The thought upon this discovery was that there was some sort of bound state forming between the impurity and the conduction electrons, which was made possible by the increasingly large coupling. In the following section, we will explore some variational methods applied to this problem, and we will find that this bound state is precisely the one that is most likely, and we will gain some more of a qualitative understanding of what is happening at low energy.

## 3 Variational Methods

One thing that we can do is apply variational methods to Anderson's model of the Kondo problem; as we will find, this will give us an even better picture of the physics occurring at this scale.

First, we are expecting some sort of singlet in the ground state. A trial wavefunction that represents this is:

$$|\psi_0\rangle = \left[\alpha_0 + \sum_{k<k_F,\sigma} \alpha_{\mathbf{k}} c_{d,\sigma}^\dagger c_{\mathbf{k},\sigma}\right]|0\rangle\,. \tag{3.1}$$

The ket $|0\rangle$ represents a filled Fermi sea of conduction electrons, with $\alpha_0$ its amplitude. The other term in brackets represents all the possible combinations of excitations of an electron from the Fermi sea to the impurity site; this is exactly our singlet we are considering. We now consider the variational energy functional

$$\tilde{E}[|\psi_0\rangle] = \frac{\langle\psi_0|\hat{H}|\psi_\rangle\rangle}{\langle\psi_0|\psi_0\rangle}, \tag{3.2}$$

where we are using the Anderson model's Hamiltonian:

$$\hat{H} = \epsilon_d n_d + U n_{d,\uparrow} n_{d,\downarrow} + \sum_{\mathbf{k},\sigma} c_{\mathbf{k},\sigma}^\dagger c_{\mathbf{k},\sigma} + \sum_{\mathbf{k},\sigma}\left(V_{\mathbf{k}} c_{\mathbf{k},\sigma}^\dagger d_\sigma + V_{\mathbf{k}}^* d_\sigma^\dagger c_{\mathbf{k},\sigma}\right). \tag{3.3}$$

Here, $\epsilon_d$ is the occupation energy of the $d$-orbital of the impurity, $n_d = \sum_\sigma \epsilon_d d_\sigma^\dagger d_\sigma$ with $d^{(\dagger)}$ being the creation/annihilation operators for the impurity, $c^{(\dagger)}$ are the creation/annihilation operators for the Bloch states of the conduction electrons, and $V$ is the hybridization. Importantly, there is a potential term denoted $U$, which represents the Coulomb interaction between the two electrons in a doubly occupied $d$-orbital.

By plugging our trial wavefunction and Hamiltonian into the variational energy functional, we find:

$$\tilde{E} = 2\sum_{k<k_F} \frac{|V_{\mathbf{k}}|^2}{\tilde{E} - \epsilon_d + \epsilon_{\mathbf{k}}}. \tag{3.4}$$

If we now define the *binding energy* $\Delta_K \equiv \tilde{E} - \epsilon_d$, we can write

$$\epsilon_d + \Delta_K = 2\sum_{k<k_F} \frac{|V_{\mathbf{k}}|^2}{\Delta_K - |\epsilon_{\mathbf{k}}|}, \tag{3.5}$$

where, since we are measuring all energies relative to the Fermi surface, we know that $\epsilon_{\mathbf{k}} < 0$, meaning we can write it as $-|\epsilon_{\mathbf{k}}|$. Now, we can convert this to the continuum in $k$, and if we assume that the hybridization $V$ is independent of $k$, we get

$$\epsilon_d + \Delta_K = 2\rho \int_0^{\epsilon_F} \mathrm{d}\epsilon \, \frac{-|V|^2}{\epsilon - \Delta_K} \tag{3.6}$$

$$= -2\epsilon |V|^2 \ln\left(\frac{\epsilon_F}{|\Delta_K|}\right). \tag{3.7}$$

Our last assumption we can make is that the occupation energy of the $d$-orbital is much larger than the binding energy. In this case, we can neglect it from the left of Eq. (3.7) and solve for it on the right to find

$$\Delta_K = -\epsilon_F \exp\left[-\frac{1}{2\rho J}\right], \tag{3.8}$$

where we have taken $|V|^2/\epsilon_d \equiv J$ as the coupling term. The important realization here is that this binding energy is negative, which indicates that our trial wavefunction, representative of the singlet state, is the one that is most likely and most preferable for the system to be in.

To go further, since this bound state is the most preferable, we would expect that $\langle n_d \rangle = 1$ in the case of a strong on-site potential/repulsion term $U$. In fact, calculating this, we find that

$$1 - \langle n_d \rangle \approx \frac{\pi \Delta_K}{2\Delta} \ll 1 \neq 0, \tag{3.9}$$

where $\Delta$ is the resonance width of the $d$-orbital. Interestingly, it is very small but not equal to one, indicating a slightly less than unity occupation. This means that there is going to be an excess of states at the Fermi surface, which corresponds to the **Kondo resonance**; see Fig. 3.1.

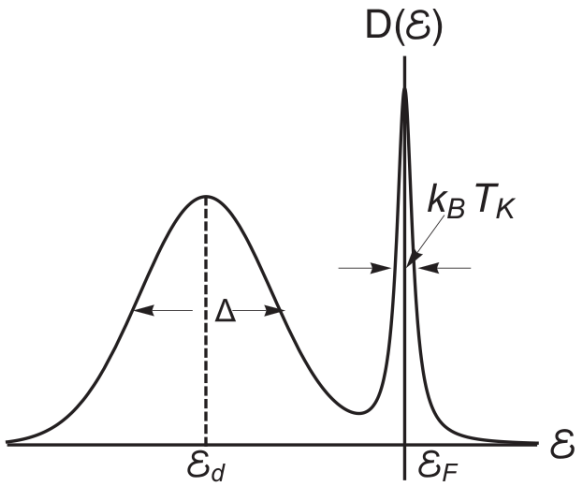


Figure 3.1: Schematic of the appearance of a Kondo resonance at the Fermi surface.

With this in mind, we can make the realization that the increased density of states is going to form a scattering center for the other conduction electrons, allowing another form of energy dissipation as the electron-phonon scattering will decrease. This explains why, after a certain temperature, the resistance starts increasing again: there is a minimum at the point when the electron-phonon interactions are very low but no singlet has formed; but, once the singlet *does* form, it provides another means of scattering which will hence begin increasing the resistance again as the Kondo resonance becomes more peaked. This goes back to the Kondo cloud picture given in Fig. 1.2.

# 4 The Numerical Renormalization Group Approach

Now that we have understood the qualitative picture of what the physics looks like, we can being to discuss the NRG proposed by Wilson which finally yielded correct results at low energies. We start, first, with some generic information about what the renormalization group is, then we will get into Wilson's application of it to the Kondo problem.

## 4.1 The Renormalization Group

In the most general way, the renormalization group is a mapping of one Hamiltonian consisting of one set of parameters to a Hamiltonian of the same form with a "renormalized" set of parameters, valid at a new energy scale. Denoting the original set of parameters as $\mathbf{K}$ and the renormalized as $\mathbf{K}'$, we can write this as:

$$\mathcal{R}_\alpha[\hat{H}(\mathbf{K})] = \hat{H}(\mathbf{K}'), \tag{4.1}$$

or equivalently:

$$\mathcal{R}_\alpha(\mathbf{K}) = \mathbf{K}'. \tag{4.2}$$

This renormalization is characterized by a parameter $\alpha$ which is related to the ratio of the energy scales between the two sets of parameters. Applying many subsequent transformations forms a *trajectory* for the parameters. In this application, this is done by reducing the energy scale for successive transformations.

A *fixed point* in parameter space is a set of parameters $\mathbf{K}^*$ which remains invariant under a renormalization group transformation; i.e. it maps the Hamiltonian onto itself:

$$\mathcal{R}[\hat{H}(\mathbf{K}^*)] = \hat{H}(\mathbf{K}^*). \tag{4.3}$$

We can linearize the transformation (which is otherwise, in general, not linear) around this fixed point for some $\mathbf{K} = \mathbf{K}^* + \delta\mathbf{K}$, after which we can expand around the fixed point:

$$\mathcal{R}_\alpha(\mathbf{K}^* + \delta\mathbf{K}) = \mathbf{K}^* + \mathbf{L}^*_\alpha \delta\mathbf{K} + \mathcal{O}(\delta\mathbf{K}^2). \tag{4.4}$$

From here, if we know the eigenvectors and eigenvalues of $\mathbf{L}^*_\alpha$ and make the assumption that they are complete, they can be used as a basis for $\delta\mathbf{K}$. Then, we are able to write (discarding higher order contributions) an equation for the application of $\mathcal{R}_\alpha$ on the region around the fixed point:

$$\mathcal{R}_\alpha(\mathbf{K}^* + \delta\mathbf{K}) = \mathbf{K}^* + \sum_n (\delta K)_n \lambda^*_n \mathbf{E}^*_n, \tag{4.5}$$

where $(\delta K)_n$ are the components of $\delta\mathbf{K}$, and $\lambda^*_n$ and $\mathbf{E}^*_n$ are the eigenvectors and eigenvalues of $\mathbf{L}^*$. In general, this transformation can be applied $m$ times:

$$\mathcal{R}^m_\alpha(\mathbf{K}^* + \delta\mathbf{K}) = \mathbf{K}^* + \sum_n (\delta K)_n (\lambda^*_n)^m \mathbf{E}^*_n, \tag{4.6}$$

There are different classifications for the values that the eigenvalues can take, but their names are not particularly relevent for the scope of this project. What is important, though, is the fact that we are able to describe the behavior in a region around the fixed point by using the effective Hamiltonian for that fixed point. Anderson's poor man's scaling approach was essentially done in this way by successively reducing the energy scale of the conduction band – the parameter $\alpha$ would relate the successive energy scales. His set of parameters consisted only of the coupling $J$ between the impurity spin and the conduction electron spins. In the antiferromagnetic case, we can notice that $J \to \infty$ is one such fixed point. Our goal (Wilson's goal, rather), then, phrased in terms of the Anderson model, is to apply this approach such that we determine the effective Hamiltonian for this fixed point. We can then use this effective Hamiltonian to determine behavior near the fixed point, and then make calculations of thermodyamic quantities such as the resistivity.

In principle, we are able to determine the exact forms of these effective Hamiltonians, from which we can make these additional calculations. I was unable to fully explore this side of things, but found it valuable to describe fixed points and effective Hamiltonians because they are the means by which the results

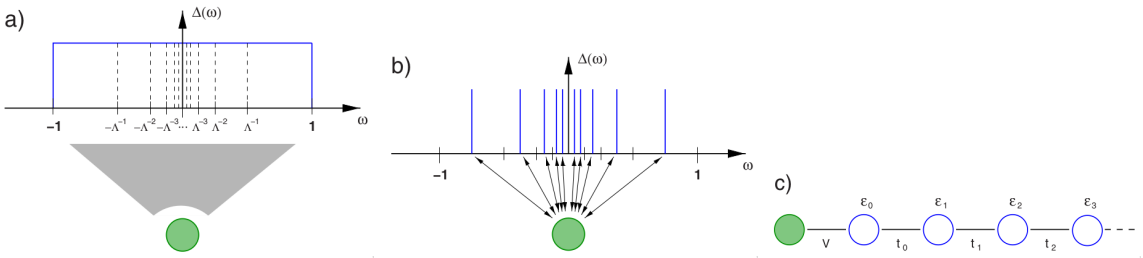


(a) Logarithmic binning. (b) Discretization. (c) Mapping to linear chain.

Figure 4.1: Diagrammatical representation of the main steps involved in the NRG procedure.

are calculated with higher accuracy. The renormalization group method itself, as we will see, is still very effective, but does carry some error as its starting point is a Hamiltonian effective at a much higher energy scale (that being whatever the initial energy scale is chosen to be for the evolution). It is then progressively rescaled, but still retains its original form. Again, this works very well: however by determining the exact form of the effective Hamiltonians at the $J \to \infty$ fixed point would, in principle, let us make more accurate calculations.

## 4.2 The Numerical Renormalization Group

With this, we can now explore the main part of this project: the NRG. It is worth pointing out, though, that this method is highly specialized to this application, i.e. the Anderson impurity model – it is an immensely challenging problem and thus some generic methods just simply don't work. With this, the general steps for the NRG procedure are:

1. Divide the energy spectrum into logarithmic bins via a parameter $\Lambda > 1$, giving positive and negative energy intervals $[\Lambda^{-(n+1)}, \lambda^{-n}]$ and $[-\Lambda^{-n}, -\lambda^{-(n+1)}]$, as in Fig. 4.1a.

2. Pick a single characteristic state from within each continuous interval, such that we have a discrete set of states (separated logarithmically), as in Fig. 4.1b.

3. Map these continuous states onto a semi-infinite linear chain with the impurity site placed at one end, as in Fig. 4.1c.

4. Iteratively diagonalize the resulting Hamiltonian after adding subsequent conduction sites to the end of the linear chain.

The reason as to why we are doing it this way, i.e. ultimately mapping onto a chain, is because of the fact that adding subsequent sites is a relatively easy thing to do computationally as it is inherently iterative. Further, as we will see later on, we can utilize symmetries of the problem in order to reduce the size of the matrices that we have to diagonalize, since they would in principle grow exponentially based on the dimension of the added basis of the new site. This makes their computation significantly easier, rendering this technique very useful.

One question that may be asked is how this pertains to a renormalization group transformation at each step. In particular, our goal is to resolve the low energy behavior of our system further and further each iteration, leaving us with an effective Hamiltonian valid at each new energy scale. The iterative step involves adding a new site to the end of the chain, which interacts with the one before it via the hopping term $t_n$. As we will find out, the logarithmic discretization leads to these terms being proportional to $\Lambda^{-n/2}$. Therefore, the interpretation of the added site is that we are accessing an new energy scale that is reduced by a factor of $\sqrt{\Lambda}$. This is the essence of the NRG; it will be reiterated once we have all the pieces.

### 4.2.1 Logarithmic Discretization

To reiterate, Anderson's model describes the impurity as a localized moment formed by a Coulomb interaction $U$ between two electrons. The total Hamiltonian, including the sum of the contributions from the impurity, the bath, and the interaction between the two is given by[2]

$$\hat{H} = \hat{H}_{\text{imp}} + \hat{H}_{\text{bath}} + \hat{H}_{\text{int}} \tag{4.7}$$

$$= \sum_{\sigma} \epsilon_f \hat{f}_{\sigma}^{\dagger} \hat{f}_{\sigma} + U \hat{f}_{\uparrow}^{\dagger} \hat{f}_{\uparrow} \hat{f}_{\downarrow}^{\dagger} \hat{f}_{\downarrow} + \sum_{k,\sigma} \epsilon_k \hat{c}_{k\sigma}^{\dagger} \hat{c}_{k\sigma} + \sum_{k,\sigma} V_k (\hat{f}_{\sigma}^{\dagger} \hat{c}_{k,\sigma} + h.c.), \tag{4.8}$$

where the $f$ operators create impurity states with energy $\epsilon_f$, the $c$ operators create bath states with energies $\epsilon_k$, and $V_k$ is a hybridization term. (Hats will be dropped from operators from here on out.) The physical quantity related to the influence of the bath of conduction states on the impurity is determined by the *hybridization function* $\Delta(\omega)$, given by

$$\Delta(\omega) = \pi \sum_{k} V_k^2 \delta(\omega - \epsilon_k). \tag{4.9}$$

Since this is a *physical* quantity, we want to ensure that its form remains the same after doing the following transformations. One such transformation that we can do is to bring the bath and interaction components into the continuum:

$$\hat{H} = \hat{H}_{\text{imp}} + \sum_{\sigma} \int_{-1}^{1} \mathrm{d}\epsilon \; g(\epsilon) a_{\epsilon\sigma}^{\dagger} a_{\epsilon\sigma} + \sum_{\sigma} \int_{-1}^{1} \mathrm{d}\epsilon \; h(\epsilon) (f_{\sigma}^{\dagger} a_{\epsilon\sigma} + a_{\epsilon\sigma}^{\dagger} f_{\sigma}), \tag{4.10}$$

with $g(\epsilon)$ being the dispersion and $h(\epsilon)$ being the hybridization, which are now continuous. These new $a$ operators satisfy standard fermionic commutation relations, and we have also imposed energy cutoffs at $\epsilon = \pm 1$ (i.e. by imposing a bandwidth of $[-1, 1]$).

We may now define our parameter $\Lambda$, which will serve to discretize our energy spectrum:

$$x_n = \pm \Lambda^{-n}, \quad n = 0, 1, 2, \ldots, \tag{4.11}$$

with the width of each interval determined by

$$d_n = \Lambda^{-n}(1 - \Lambda^{-1}). \tag{4.12}$$

Of course, we must have $\Lambda > 1$. Inside of each interval, we can now define a complete set of orthonormal functions which are simply plane waves with characteristic frequency determined simply by $\omega_n = 2\pi/d_n$ (and normalized to the interval width):

$$\psi_{np}^{\pm}(\epsilon) = \begin{cases} \frac{1}{\sqrt{d_n}} e^{\pm i \omega_n p \epsilon}, & \text{for } x_{n+1} < \epsilon < x_n, \text{ and} \\ 0 & \text{otherwise,} \end{cases} \tag{4.13}$$

where $p \in \mathbb{Z}$. We can expand the original $a$ operators in this new basis like so:

$$a_{\epsilon\sigma} = \sum_{np} \left( a_{np\sigma} \psi_{np}^{+}(\epsilon) + b_{np\sigma} \psi_{np}^{-}(\epsilon) \right), \tag{4.14}$$

At this point, by using the $a_{\epsilon,\sigma}$ operators, we now have expressed our Hamiltonian from Eq. (4.10) in terms of discrete creation and annihilation operators for states residing within each logarithmic band. To assist with notation for the following steps, we define:

$$\int^{+n} \mathrm{d}\epsilon \equiv \int_{x_{n+1}}^{x_n} \mathrm{d}\epsilon, \quad \text{and} \quad \int^{-n} \mathrm{d}\epsilon \equiv \int_{-x_n}^{-x_{n+1}} \mathrm{d}\epsilon. \tag{4.15}$$

[2]Note the change of notation here compared to that in Sec. 3; the creation/annihilation operators for the $d$-level of the impurity are now represented by $f$s. This is to reflect what is seen in the literature and code documentation. Also, in principle, it is the $f$-orbitals in heavy fermions which are more strongly interacting.

With this, we can express the hybridization term of our quasi-continuous Hamiltonian like so:

$$\int_{-1}^{1} \mathrm{d}\epsilon\; h(\epsilon) f_\sigma^\dagger a_{\epsilon\sigma} = f_\sigma^\dagger \sum_{np} \left[ a_{np\sigma} \int^{+n} \mathrm{d}\epsilon\; h(\epsilon)\psi_{np}^{+}(\epsilon) + b_{np\sigma} \int^{-n} \mathrm{d}\epsilon\; h(\epsilon)\psi_{np}^{-}(\epsilon) \right], \tag{4.16}$$

where the other term will of course just be the conjugate. It is here we make one important assumption: that the hybridization $h(\epsilon)$ remain constant within each band, i.e. that $h(\epsilon) = h$. If we make this assumption, then the above integrals actually filter out only the $p = 0$ state:

$$\int^{\pm n} \mathrm{d}\epsilon\; \psi_{np}^{\pm}(\epsilon) = \sqrt{d_n} h \delta_{p,0}, \tag{4.17}$$

which has the physical implication that the impurity states only couple to the $p = 0$ conduction states.[3] We could have also imposed this fact instead, which would have led to a constant hybridization. These are equivalent, and they are the defining assumption from Wilson's technique. Now, we can make a further assumption with the hybridization: it is defined as a sort of *step* function where it is equal to the average of the hybridization function over that interval:

$$h(\epsilon) = h_n^{\pm}, \quad x_{n+1} < \pm\epsilon < x_n, \tag{4.18}$$

where

$$h_n^{\pm 2} = \frac{1}{d_n} \int^{\pm n} \mathrm{d}\epsilon\; \frac{\Delta(\epsilon)}{\pi}. \tag{4.19}$$

With this in mind, the hybridization term in our Hamiltonian turns out to be:

$$\int_{-1}^{1} \mathrm{d}\epsilon\; h(\epsilon) f_\sigma^\dagger a_{\epsilon\sigma} = \frac{1}{\pi} f_\sigma^\dagger \sum_n \left( \gamma_n^{+} a_{n0\sigma} + \gamma_n^{-} b_{n0\sigma} \right), \tag{4.20}$$

where the $\gamma$ terms are given by

$$\gamma_n^{\pm 2} = \int^{\pm n} \mathrm{d}\epsilon\; \Delta(\epsilon). \tag{4.21}$$

We can now do the same for the conduction electron term:

$$\int_{-1}^{1} \mathrm{d}\epsilon\; g(\epsilon) a_{\epsilon\sigma}^\dagger a_{\epsilon\sigma} = \sum_{np} \left( \xi_n^{+} a_{np\sigma}^\dagger a_{np\sigma} + \xi_n^{-} b_{np\sigma}^\dagger b_{np\sigma} \right) \tag{4.22}$$

$$+ \sum_{n, p \neq p'} \left[ \alpha_n^{+}(p,p') a_{np\sigma}^\dagger a_{np'\sigma} - \alpha_n^{-}(p,p') b_{np\sigma}^\dagger b_{np'\sigma} \right]. \tag{4.23}$$

The first term on the right is already diagonal in $p$; it turns out we can hence express the eigenvalues $\xi$ as

$$\xi_n^{\pm} = \frac{\int^{\pm} \mathrm{d}\epsilon\; \Delta(\epsilon)\epsilon}{\int^{\pm} \mathrm{d}\epsilon\; \Delta(\epsilon)}. \tag{4.24}$$

If we assume a constant $\Delta(\epsilon)$, then this simplifies to

$$\xi_n^{\pm} = \frac{1}{2}\Lambda^{-n}(1 + \Lambda^{-1}) = \frac{d_n}{2}. \tag{4.25}$$

In the case of a linear dispersion term, i.e. $g(\epsilon) = \epsilon$, we can determine the form of the $\alpha$ prefactors in Eq. (4.23):

[3] This relation can be very easily shown using the definition of the basis states.

$$\alpha_n^{\pm}(p,p') = \frac{1-\Lambda^{-1}}{2\pi i}\frac{\Lambda^{-n}}{p'-p}\exp\frac{2\pi i(p'-p)}{1-\Lambda^{-1}}. \tag{4.26}$$

Here we can make a bit of a better argument for the dropping of $p \neq 0$ terms. The $\alpha$ prefactors contain a term like $1-\Lambda^{-1}$, which, in the continuum limit where $\Lambda \to 1$, will go to zero. It is through these that the $p \neq 0$ terms interact with the $p = 0$ term. We can hence treat any terms above $p = 0$ as a *perturbation* to the $p = 0$ term; if we consider just leading order, this involves dropping the $p \neq 0$ terms. It may seem like a crude approximation, but it turns out to work very well even for moderately large values of $\Lambda$, such as 2 or 3.[4]

So, dropping all $p \neq 0$ terms, we will have fully achieved the logarithmic discretization of the Hamiltonian:

$$\hat{H} = \hat{H}_{\text{imp}} + \sum_{n\sigma}\left(\xi_n^+ a_{n\sigma}^\dagger a_{n\sigma} + \xi_n^- b_{n\sigma}^\dagger b_{n\sigma}\right) \tag{4.27}$$

$$+ \frac{1}{\sqrt{\pi}}\sum_\sigma f_\sigma^\dagger \sum_n \left(\gamma_n^+ a_{n\sigma} + \gamma_n^- b_{n\sigma}\right) \tag{4.28}$$

$$+ \frac{1}{\sqrt{\pi}}\sum_\sigma \left(\sum_n \left(\gamma_n^+ a_{n\sigma}^\dagger + \gamma_n^- b_{n\sigma}^\dagger\right)\right) f_\sigma. \tag{4.29}$$

### 4.2.2 Mapping to Semi-Infinite Linear Chain

Our next goal is to map this discretized Hamiltonian onto a semi-infinite chain with the impurity placed at the first site. This means we will have the impurity connected to only a single conduction electron with operators $c_{0\sigma}^{(\dagger)}$, and we will have hopping terms connecting the bath states. We can determine the form of the $c_{0\sigma}^{(\dagger)}$ operators from our final expression for the discretized Hamiltonian:

$$c_{0\sigma} = \frac{1}{\sqrt{\xi_0}}\sum_n \left(\gamma_n^+ a_{n\sigma} + \gamma_n^- b_{n\sigma}\right), \tag{4.30}$$

with normalization

$$\xi_0 = \sum_n \left[(\gamma_n^+)^2 + (\gamma_n^-)^2\right] = \int_{-1}^{1} \mathrm{d}\epsilon\, \Delta(\epsilon). \tag{4.31}$$

In terms of $c_{0\sigma}$, the hybridization term can be written like

$$\frac{1}{\sqrt{\pi}} f_\sigma^\dagger \sum_n \left(\gamma_n^+ a_{n\sigma} + \gamma_n^- b_{n\sigma}\right) = \sqrt{\frac{\xi_0}{\pi}} f_\sigma^\dagger c_{0\sigma}, \tag{4.32}$$

and the $c_{0\sigma}^\dagger$ operator follows similarly. After doing this, we find that our chain Hamiltonian looks like:

$$\hat{H} = \hat{H}_{\text{imp}} + \sqrt{\frac{\xi_0}{\pi}}\sum_\sigma \left(f_\sigma^\dagger c_{0\sigma} + c_{0\sigma}^\dagger f_\sigma\right) = \hat{H}_{\text{imp}} + \sum_{\sigma n=0}^{\infty}\left[\epsilon_n c_{n\sigma}^\dagger c_{n\sigma} + t_n\left(c_{n\sigma}^\dagger c_{n+1\sigma} + c_{n+1\sigma}^\dagger c_{n\sigma}\right)\right], \tag{4.33}$$

where the $t_n$'s are the hopping matrix elements, determined by:

$$t_n = \Lambda^{-n/2}\frac{(1+\Lambda^{-1})(1-\Lambda^{-n-1})}{2\sqrt{1-\Lambda^{-2n-1}}\sqrt{1-\Lambda^{-2n-3}}}. \tag{4.34}$$

[4] Most of this section has come from Refs. [6] and [7] and isn't particularly groundbreaking, hence the lack of individual citations; this, however, is a bit of a interesting result, so I directly cite these two here for a bit of an exploration on this approximation. Further, Wilson's original paper [5] contains some commentary on it.

### 4.2.3 Connection to Renormalization Group

Now, here is where the NRG really enters (after all, what we've done so far is nothing more than some mappings/transformations). The interpretation of this Hamiltonian is that it can be viewed as a series of Hamiltonians $H_N$ that approach the original Hamiltonian for $H \to \infty$. More specifically:

$$H = \lim_{N\to\infty} \Lambda^{-(N-1)/2} H_N, \tag{4.35}$$

with

$$\begin{aligned} H_N = \Lambda^{(N-1)/2} \Bigg[ & H_{\text{imp}} + \sqrt{\frac{\xi_0}{\pi}} \sum_\sigma \left( f_\sigma^\dagger c_{0\sigma} + c_{0\sigma}^\dagger f_\sigma \right) \\ & + \sum_{\sigma n=0}^{N} \epsilon_n c_{n\sigma}^\dagger c_{n\sigma} + \sum_{\sigma n=0}^{N-1} t_n \left( c_{n\sigma}^\dagger c_{n+1\sigma} + c_{n+1\sigma}^\dagger c_{n\sigma} \right) \Bigg], \end{aligned} \tag{4.36}$$

where the $n$ sums now go to $N$, corresponding to the number of bath states on the chain for that iteration. The scaling factor in Eq. (4.36) serves to cancel that in Eq. (4.35); notably, the $\Lambda$ dependence still remains in the hopping terms $t_n$ as well as the recursion relation for subsequent $H_N$s which is given by

$$H_{N+1} = \sqrt{\Lambda} H_N + \Lambda^{N/2} \sum_\sigma \epsilon_{N+1} c_{N+1\sigma}^\dagger c_{N+1\sigma} + \Lambda^{N/2} \sum_\sigma t_N \left( c_{N\sigma}^\dagger c_{N+1\sigma} + c_{N+1\sigma}^\dagger c_{N\sigma} \right). \tag{4.37}$$

The starting point, denoted $H_0$, has the form

$$H_0 = \Lambda^{-1/2} \left[ H_{\text{imp}} + \sum_\sigma \epsilon_0 c_{0\sigma}^\dagger c_{0\sigma} + \sqrt{\frac{\xi_0}{\pi}} \sum_\sigma \left( f_\sigma^\dagger c_{0\sigma} + c_{0\sigma}^\dagger f_\sigma \right) \right]. \tag{4.38}$$

This initial Hamiltonian is representative of the single two-electron impurity state and the first conduction electron. What this really is is a renormalization group transformation. In particular, the mapping from $H_N$ to $H_{N+1}$ is understood as $H_{N+1}(\mathbf{K}) = \mathcal{R}[H_N(\mathbf{K})]$. In principle, then, we can diagonalize $H_0$, then repeatedly add sites and diagonalize the resulting Hamiltonian up to a satisfactory number of iterations. However, as we will see in Sec. 4.4, our particular choice of basis means that the dimension of the Hamiltonian grows exponentially for each added site. From our logarithmic discretization in the previous section, we found that it resulted the hopping terms $t_n \propto \Lambda^{-n/2}$. This, as described earlier, results in the accessing of lower energy scales, which is the main goal of the method. But what it also implies is that any higher energy effects associated with accessing those states (we are accessing lower energy *levels*, but that doesn't stop other higher energy effects from *occurring*) are vanishingly weak with respect to its effect on the impurity. Therefore, we are able to truncate the resultant set of states, dropping all higher order effects and keeping the dimensionality of our problem reasonable. A little schematic is given in Fig. 4.2.

## 4.3 Calculation of Thermodynamic Quantities

Before the setting up of the problem, we briefly present the thermodynamic quantities that we can calculate and compare to those in the literature. The first thing to mention, though, is that since energy and temperature are directly related, each added site corresponds also to an accessing of lower *temperatures*. Via our scaling of the Hamiltonians and the definition of the Boltzmann factors, we have something that looks like

$$k_B T_N = \frac{1}{2}(1 + \Lambda^{-1}) \Lambda^{-(N-1)/2} / \beta. \tag{4.39}$$

For some iteration $N$, we therefore have a relation for the temperature $T_N$ for that iteration. To actually make this determination, we *choose* a value of $\beta$, then plug in $\Lambda$ and $N$ to get $T_N$. Intuitively, a high value of $\beta$ corresponds to low temperatures and a low value of $\beta$ corresponds to high temperatures. We cannot choose too high a value for $\beta$ since this would involve higher temperature effects which we are deliberately

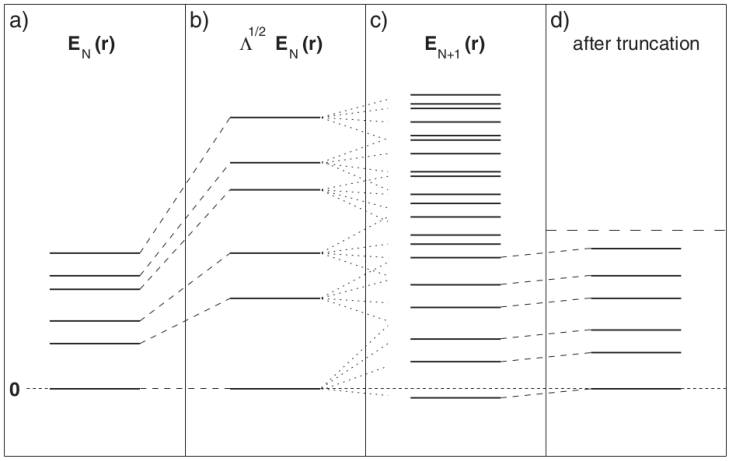


Figure 4.2: Schematic describing the truncation of states to $N_s$ total states after each iteration.

truncating after each iteration. On the other hand, we cannot choose too low a value, since we simply wouldn't have enough states/temperatures to perform a valid calculation. It turns out that a value $\sim \mathcal{O}(1)$ is suitable, in particular 0.5 to 1, or sometimes up to $\sqrt{\Lambda}$, since we take $\Lambda$ to be no greater than 3. With this choice, we are then able to determine $T_N$ and thermodynamic quantities. We took it to be 1.0 in our code.

In particular, we are interested in calculating the entropy $S$, the heat capacity $C$, and the magnetic susceptibility $\chi$:

$$S = \beta \langle H \rangle + \ln Z, \tag{4.40}$$

$$C = \beta^2(\langle H^2 \rangle - \langle H \rangle^2), \tag{4.41}$$

$$\chi = \beta(\langle S_{\mathrm{tot},z}^2 \rangle - \langle S_{\mathrm{tot},z} \rangle^2), \tag{4.42}$$

where, as standard in thermodynamics, the average of a quantity $X$ is given by

$$\langle X \rangle = \frac{1}{Z} \sum_i X_i e^{-\beta X_i}, \tag{4.43}$$

with $Z$ being the partition function. We also note that our goal is to determine the impact the impurity has on these values for a system. In order to do this, we calculate these quantities with the chain in which the impurity is placed at the beginning, as has been described, then we do the same calculates for the chain without the impurity. We subtract off the latter from the former, which yields only the effects due to the impurity.

## 4.4 Application to the Project

There are a number of additional formalities to be discussed regarding the diagonalization of the resulting chain Hamiltonians. However, in spirit of the fact that the NRG method described above is already highly specialized to the Anderson model, I feel it best to leave out the rest of those formalities and instead focus on the specifics of constructing the solutions for this project.

One of the first assumptions we can make is to assume particle-hole symmetry, which has the effect of setting occupation energies for the conductions states to zero, thereby eliminating that term from the Hamiltonian altogether. Another assumption we make is to assume a constant hybridization, meaning the factor $\sqrt{\xi_0/\pi} \to V$. With this, the initial Hamiltonian turns into, after expanding the impurity part:

$$H_0 = \Lambda^{-1/2} \left[ \sum_\sigma \epsilon_f f_\sigma^\dagger f_\sigma + U f_\uparrow^\dagger f_\uparrow f_\downarrow^\dagger f_\downarrow + V \sum_\sigma \left( f_\sigma^\dagger c_{0\sigma} + c_{0\sigma}^\dagger f_\sigma \right) \right], \tag{4.44}$$

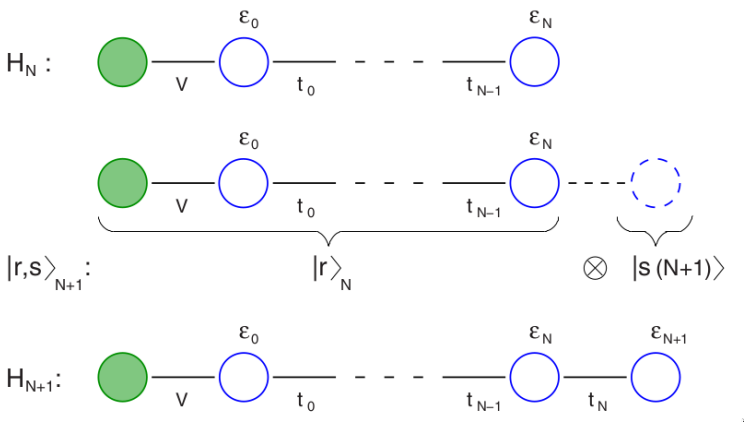


Figure 4.3: Schematic of the addition of a site to the end of the chain.

and our recursion relation becomes:

$$H_{N+1} = \sqrt{\Lambda} H_N + \Lambda^{N/2} \sum_\sigma t_N \left( c^\dagger_{N\sigma} c_{N+1\sigma} + c^\dagger_{N+1\sigma} c_{N\sigma} \right), \tag{4.45}$$

## 4.5 Initial Iteration

With this, we can begin concretely defining our basis and subsequently the actual form of our matrices so that we can diagonalize. Our choice of basis is a set of four states: empty, singly occupied with either spin up or spin down, and doubly occupied. These are denoted with $|0\rangle$, $|\uparrow\rangle$, $|\downarrow\rangle$, $|\uparrow\downarrow\rangle$ respectively. At this point, then, noticing that the impurity Hamiltonian is already diagonal, we can simply write:

$$\hat{H}_{\text{imp}} = \begin{pmatrix} 0 & 0 & 0 & 0 \\ 0 & \epsilon_f & 0 & 0 \\ 0 & 0 & \epsilon_f & 0 \\ 0 & 0 & 0 & 2\epsilon_f + U \end{pmatrix}. \tag{4.46}$$

What this is physically saying is that the unoccupied state has 0 energy, each singly occupied state has energy $\epsilon_f$, and the doubly occupied state has energy $2\epsilon_f$ (one for each electron) plus the Coulomb interaction term $U$.

Now, in the construction of the total Hamiltonian when adding the first site, we consider that the new total basis is a direct/Kronecker product of the original state (that being the impurity for the first iteration) with that of the new site. In general, for some iteration $N$, can denote its basis by $|r\rangle_N$, and the basis of the new site as $|s\rangle_{N+1}$; with this, the new basis is therefore denoted as $|r;s\rangle_{N+1} \equiv |r\rangle_N \otimes |s\rangle_{N+1}$. This is shown in Fig. 4.3.

In general, for the total Hamiltonian, we have that

$$\hat{H}_{\text{tot}} = I_4 \otimes \hat{H}_{\text{imp}} + \hat{H}_{c0} \otimes I_4 + \hat{H}_{\text{hyb}}, \tag{4.47}$$

where, since we are taking occupation energy of the conduction states to zero, we are left with just:

$$\hat{H}_{\text{tot}} = I_4 \otimes \hat{H}_{\text{imp}} + \hat{H}_{\text{hyb}}, \tag{4.48}$$

with

$$\hat{H}_{\text{hyb}} = V \sum_\sigma (c^\dagger_{0,\sigma} \otimes f_\sigma + c_{0,\sigma} \otimes f^\dagger_\sigma). \tag{4.49}$$

It is important to note the order in which the direct product is taken – for some spaces $A$ and $B$, the form of the new space formed by the direct product $A \otimes B$ will look different than the space formed by the

direct product $B \otimes A$. Of course, by switching the order of direct products of operators acting in the total space, one will get back the same results; the spaces aren't *fundamentally* changed by this, they just will *look* different.

Here, we take the first/left space in the direct product to be the conduction site, and each new conduction site will be on the left of the direct product. In principle the definition can be whatever the author would like, but by doing it this way we use the convention that, roughly speaking, the space on the left of the direct product is the "outer" or "larger" space.

To see this a bit easier, we consider the impurity site and a single conduction site, which is our first iteration. Both spaces have dimensionality of 4, leaving a $16 \times 16$ matrix. However, we can write it in terms of $4 \times 4$ block matrices. Here is where the difference between the outer and inner spaces lie: each block itself, being a $4 \times 4$ matrix, acts on the *inner* space. What this means is that supplanting a $4 \times 4$ matrix with some non-trival (i.e. not an identity) structure into the main one will have that matrix act on the inner space. Supplanting *numbers* into the main matrix, i.e. treating the main outer $4 \times 4$ matrix itself a matrix, corresponds to placing identities at those locations which is trivial in the inner space but has the effect of the main outer $4 \times 4$ acting on the outer space.[5]

With this in mind, we can go ahead and construct what the $f$ matrices look like in general (the $c$ matrices will look identical):

$$f_\uparrow^\dagger = \begin{pmatrix} 0 & 0 & 0 & 0 \\ 1 & 0 & 0 & 0 \\ 0 & 0 & 0 & 0 \\ 0 & 0 & -1 & 0 \end{pmatrix}, \quad f_\downarrow^\dagger = \begin{pmatrix} 0 & 0 & 0 & 0 \\ 0 & 0 & 0 & 0 \\ 1 & 0 & 0 & 0 \\ 0 & 1 & 0 & 0 \end{pmatrix}, \tag{4.50}$$

where the $-1$ is incurred in the construction of $f_\downarrow^\dagger$ due to the matrices' fermionic nature. Referring to our discussion a few paragraphs above, we have that the space for our first iteration is chosen such that the conduction site is the "outer" space, meaning, as a 4×4 matrix, each block acts on the impurity space and the main 4×4 matrix acts on the outer space. We present the form of the total Hamiltonian here:

$$\hat{H}_{\text{tot},0} = \begin{pmatrix} \mathcal{H}_{\text{imp}} & V f_\uparrow^\dagger & V f_\downarrow^\dagger & 0 \\ V f_\uparrow & \mathcal{H}_{\text{imp}} & 0 & V f_\downarrow^\dagger \\ V f_\downarrow & 0 & \mathcal{H}_{\text{imp}} & -V f_\uparrow^\dagger \\ 0 & V f_\downarrow & -V f_\uparrow & \mathcal{H}_{\text{imp}} \end{pmatrix}. \tag{4.51}$$

The diagonal elements, since they need to act on the impurity space, are themselves matrices; $\mathcal{H}_{\text{imp}}$ is given in Eq. (4.46). Additionally, the $f$s are matrices and therefore act on the impurity space. But, we notice $V$s placed in the same places in the main Hamiltonian as in the general form of the $f$s. This corresponds to the $c$ matrices acting on the conduction electron space; with them being placed in the same locations, multipled by $V$, we retrieve the hybrization terms.

## 4.6 Symmetry Considerations

As is customary in physics, we want to consider what symmetries are present in the model in an attempt to reduce the number of things we have to compute, or in this case, reduce the dimensionality of the Hamiltonian. Wilson [5] chose three good quantum numbers: twice the $z$-component of spin $2S_z$ (the factor of 2 to avoid halfs), the total spin $S$, and the charge $Q$, defined as the particle number with respect to half-filling. This means that $\hat{Q}\,|0\rangle = -1$, $\hat{Q}\,|\uparrow\rangle = \hat{Q}\,|\downarrow\rangle = 0$, and $\hat{Q}\,|\uparrow\downarrow\rangle = 1$. Considering all three of these symmetries greatly reduced the dimensionality of the problem, and essentially each iteration boiled down to diagonalizing a set of smaller matrices corresponding to the states that share the same set of quantum numbers.

In practice, the inclusion of the total spin as a good quantum number involved the Clebsch-Gordan coefficients, which made things a bit of a mess. Nowadays, computers are good enough that we can compute sufficient iterations quick enough using only $2S_z$ and $Q$, avoiding further complication, and this is what most modern literature uses when discussing NRG, so it is what I will use. Additionally, in the literature, only $S_z$ is written and it is understood that the actual quantity is *twice* $S_z$.

[5] My understanding of these abstract math concepts is *very* rudimentary; this is certainly not be a mathematically correct way of saying it, but it is *correct* nonetheless, and hopefully helps give a picture of what is going on.

Now, from basic quantum mechanics, we know that if an operator commutes with the Hamiltonian, it shares an eigenbasis. If we construct a new operator using $S_z$ and $Q$ such that it essentially encodes both into one, call this new operator $\hat{Y}$, we are able to write

$$\hat{Y}\hat{H}\left|\psi\right\rangle = E(\hat{Y}\left|\psi\right\rangle) \tag{4.52}$$

$$\hat{H}(\hat{Y}\left|\psi\right\rangle) = E(\hat{Y}\left|\psi\right\rangle) \tag{4.53}$$

$$= E\left(\sum_i y_i \left|Y\right\rangle_i\right), \tag{4.54}$$

where $y_i$ are the eigenvalues and $\left|Y\right\rangle_i$ are the eigenstates. The purpose of doing it this way is that many states share the same $S_z$ and $Q$, and hence $y$, meaning two things: the sum over $i$ is effectively less than the original dimensionality of $\hat{H}$, and since our goal is to determine the energy values, we need only diagonalize the resultant block matrices created for the states that share the same $y$. For example, in the first iteration consisting of the $16 \times 16$ matrix, using this method we reduce the single diagonalization of the $16 \times 16$ into a few trivial $1 \times 1$ matrices, four $2 \times 2$s, and one $4 \times 4$, which is already a huge improvement; for higher dimensionality matrices, this method becomes incredibly effective.

After doing this and obtaining a series of eigenvalues, we then sort them (and their corresponding states) from smallest to largest, then shift them such that the ground state has an energy of zero. We do this so that we can easily truncate the states corresponding to higher energies/temperatures. Since we are changing the order of the states in our basis, we must also change the $f$ and $c$ matrices to match this. This is done by simply doing:

$$c_{0,\sigma} \to \mathbf{Y}^T c_{0,\sigma} \mathbf{Y}, \tag{4.55}$$

where $Y$ is the matrix of ordered eigenvectors. Lastly, we compute the thermodynamic quantities for this iteration, and continue on to the next.

### 4.7 Subsequent Iterations

The first iteration was special since it involved the impurity hybridizing with the first conduction site. However, after that, subsequent additions of impurity sites is an identical procedure, so the entire rest of the program can be placed inside a loop at this point. Further, these steps are nearly identical to the initial iteration, with a few key differences, that being the dimensionality of the matrices we are constructing, and the inclusion of the hopping terms. We have already described in detail the construction of the block matrices and hence the total Hamiltonian for a given iteration in terms of the different subspaces. We know the form of all the moving pieces, so it should be relatively clear how to generalize this to any subsequent iteration. In principle, the only change is to replaces $V$s with $t$s in Eq. (4.51), and make $\mathcal{H}_{\text{imp}}$ be a larger matrix with the new ordered energies down the diagonal. The $f$s, which turn into the $c$s have the same form but are just larger.

## 5 Results

This was moderately easy to program and we also had this code as a reference to ensure bugs were avoided. We chose to keep $N_s = 1000$ states each iteration[6], and we picked $\Lambda = 3.0$ and do 70 iterations. We also chose two sets of values for $\epsilon_f$, $U$, and $V$, corresponding to the impurity occupation energy, the impurity onsite repulsion $U$, and hybridization $V$. For both, we set $2\epsilon_f + U = 0$; this choice is often called the *symmetric Anderson model*. $V$ was kept fixed at $4 \times 10^{-4}$, and $U$ was set to $10^{-3}$ and $10^{-2}$.

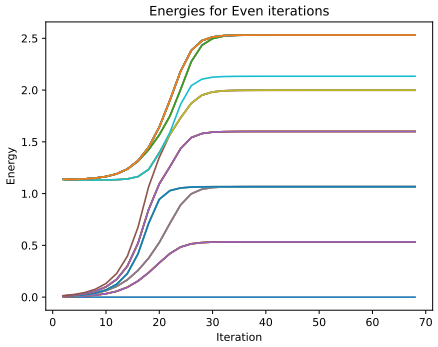


(a) Even iterations.

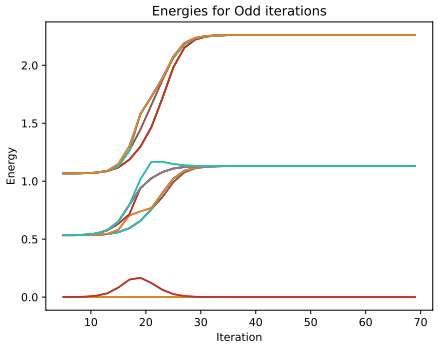


(b) Odd iterations.

Figure 5.1: Energy flows for $|U| \sim V$.

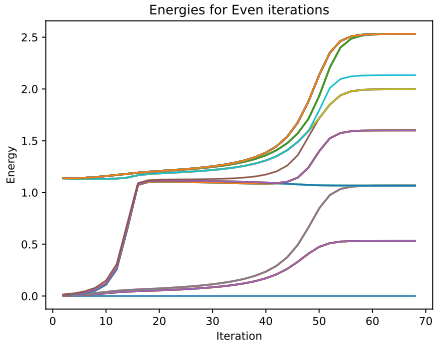


(a) Even iterations.

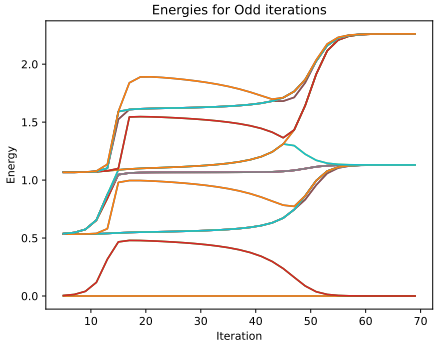


(b) Odd iterations.

Figure 5.2: Energy flows for $|U| \gg V$

## 5.1 Energy Flows

In Figs. 5.1a and 5.1b are the energy flows for the case where we took $|2\epsilon_f| \sim |U| \sim V$, i.e. we set all variables roughly equivalent. One important to notice is that there is a crossover at around 18 iterations between stable flows. This is related to the fixed points described in Sec. 4.1; lower iterations correspond to higher temperatures, so the stability observed in the first 18 iterations is related to the fact that at high energies, thermal fluctuations and other effects dominate over anything related to the impurity: it's just a free moment. However, right at the point where the singlet begins to form, we have the crossover to another fixed point related to the very large coupling limit where we have the singlet.

To explore this further, we took $U$ to be 10 times larger, and the results are given in Figs. 5.2a and 5.2b. This time we have two crossovers; the first one no longer is related to the crossover directly to the singlet, but rather a weakly coupled local moment, where due to the high repulsion and occupation energy, it's a bit harder to kick a conduction electron from the Fermi sea to form the bound state. After a while, though, we do notice this occur since we have the second crossover. We notice this behavior with all of the thermodynamic quantities, too.

[6]This is a very large number when you consider we are attempting to diagonalize 1000×1000 matrices. Evidently, both computing efficiency and our symmetry considerations are very powerful.

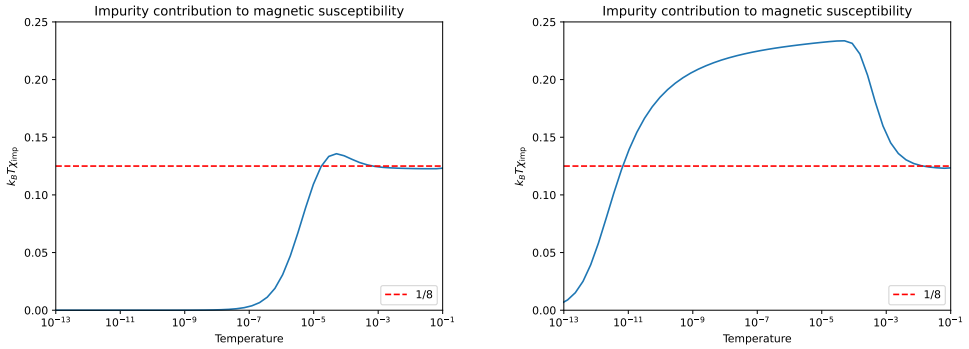


(a) Magnetic susceptibility flow for $|U| \sim V$. (b) Magnetic susceptibility flow for $|U| \gg V$.

## 5.2 Magnetic Susceptibility

Before looking at the magnetic susceptibility flows, we want to make sure we retrieve what we expect to retrieve. In particular, we know that the form of the magnetic susceptibility goes like[7]

$$\chi_{\text{imp}}(T) = \frac{(g\upsilon_B)^2}{4K_BT[1+\exp(-U/2k_BT)]}, \tag{5.1}$$

or, taking $(g\upsilon_B) \to 1$ to go unitless, we have

$$k_BT\chi_{\text{imp}}(T) = \frac{1}{4(1+e^{-U/2k_BT})}. \tag{5.2}$$

We can notice immediately that in the high temperature limit where $T \gg U$, we would have the susceptibility approach $k_BT\chi_{\text{imp}}(T) \to 1/8$, and in the other limit we would expect it to vanish; this is exactly what we observe, if we examine Figs. 5.3a and 5.3b. This is also physically what we expect: in the high coupling limit, the induced spin density fully compensates the spin of the singlet, so there should be no residual spin/magnetization remaining.

Interestingly, we notice the same crossover points as with the energy flows. Fig. 5.3a is the plot for $|U| \sim V$, where there is only one crossover between the free moment and the strongly coupled singlet. However, in Fig. 5.3b, where $U$ was taken to be 10 times larger, we notice the second crossover. In the limit for strong $U$, we would have, from Eq. (5.2), that $k_BT\chi_{\text{imp}} \approx 1/4$ for this region, which is close to what we found. It would be tough to get exactly $1/4$ since at this scale we don't necessarily have $U \gg T$, meaning the exponential isn't vanishingly small, but we can see that it is close and reproduces what we expect.

## 5.3 Entropy

In the case of entropy, we know that it has the form $S = k_B \ln \Omega$, where $\Omega$ is the multiplicity of the system. In our case, we can first easily note that in the case of the singlet, there is really only one possible way to organize the system. Therefore, the multiplicity is 1 so $S = k_B \ln 1 = 0$, which is what we observe in Figs. 5.4a and 5.4b. Further, in the free local moment, there should be 2 ways to organize that, either a spin up or spin down, meaning we would expect it to go like $\ln 2$, which it also does.

Further, just as with the energy flows and magnetic susceptibility, we notice the appearance of the weakly coupled local moment fixed point for large $U$. Unfortunately, my knowledge of thermal physics and statistical mechanics is a little lacking to explain the exact reason for an apparently non-integer multiplicity, but it is good that there is still the appearance of this fixed point, it further solidifies the fact that there is a weakly coupled local moment in the high $U$ case.

[7] See Ref. [7], for instance.

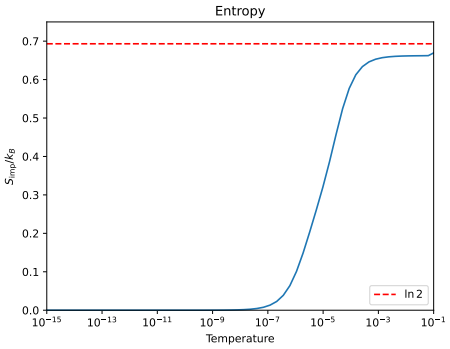


(a) Entropy flow for $(2\epsilon_f = -U) \sim V$.

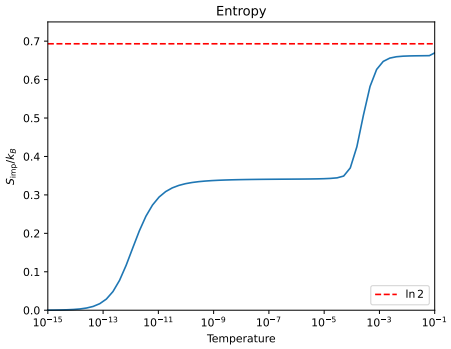


(b) Entropy flow for $(2\epsilon_f = -U) \gg V$.

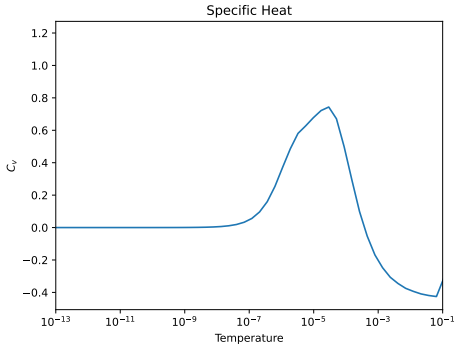


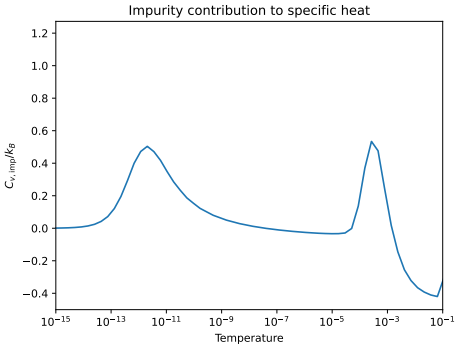


(a) Flow of heat capacity for $(2\epsilon_f = -U) \sim V$. (b) Flow of heat capacity for $(2\epsilon_f = -U) \gg V$.

### 5.4 Heat Capacity

For the heat capacity, we expect for the contribution from the impurity to vanish in both limits, i.e. when it is both a perfectly free moment and when it is a Kondo singlet. We also notice that are peaks at the crossover points; wo find one peak in the $|U| \sim V$ case as in Fig. 5.5a and two peaks in the large $U$ case as in Fig. 5.5b. Unfortunately, again, I do not know enough to explain the behavior apart from this.

It is definitely interesting, though, that it *peaks* at the crossover points and remains roughly zero everywhere else. Perhaps this could have something to do with "phase transitions"; of course they aren't actually phase transitions, but maybe the behavior is related.

## 6 Discussion and Conclusions

To summarize, I was able to implement the NRG applied to the single-impurity Anderson model and get some results out that matched that of the papers at the time, namely Refs. [5], [8], and more recently [6]. The programming implementation was fortunately not too challenging due to, as mentioned earlier, the reference code. The thermodynamic results (the ones that I was able to fully understand) also matched with what was found in the papers as well as basic physics understanding. Hence, I have confirmed the physical picture that the magnetic impurity, at low energy scales, forms a singlet with the conduction electrons, called the Kondo singlet, which provides a residual scattering center within the metal that serves to increase the resistivity.

Had I more time, I would have liked to explore further the idea of the effective Hamiltonians at the fixed points. This was mentioned before, but by determining the forms of the effective Hamiltonians at the different fixed points, we'd be able to calculate things with much higher precision. The forms themsleves would also give a little bit of intuition into the physics of the problem. The Kondo problem was a bit too complex, though, so I didn't quite have enough time to do this.

Despite this, there are a few ways to improve accuracy even without effective Hamiltonians; one such

method is called $z$-averaging. This involves running the program multiple times and essentially replacing $\Lambda^{-n}$ with $\Lambda^{-n-z}$ for different $z$ values. It turns out that even with only a couple different $z$ values the accuracy already improves tremendously, so this would have been good to implement, but I simply didn't have enough time.

Lastly, the NRG can obviously be applied to other models, such as the original Kondo model, or asymmetric Anderson model, albeit with some modifications. It would have been nice to implement NRG for these models to get an idea of the different type of physics they describe.

Overall, the Kondo problem is an insanely challenging problem, and only after over a decade's worth of research was the NRG finally formulated by Wilson, but only for the single-impurity Anderson model, the one studied in this project. More complicated systems took even longer, and even nowadays it is still a highly researched model. One model of note that I came across is the Kondo lattice; I know nothing about it obviously, but it goes to show that the Kondo problem is still being worked on after over half a century later: there is so much rich physics to discover related to impurities within metals.

# References


[1] W. Meissner and B. Voigt, "Messungen mit hilfe von flüssigem helium xi widerstand der reinen metalle in tiefen temperaturen," en, *Annalen der Physik*, vol. 399, no. 8, pp. 892–936, Jan. 1930, ISSN: 0003-3804, 1521-3889. DOI: 10.1002/andp.19303990803.

[2] W. De Haas and G. Van Den Berg, "The electrical resistance of gold and silver at low temperatures," en, *Physica*, vol. 3, no. 6, pp. 440–449, Jun. 1936, ISSN: 00318914. DOI: 10.1016/S0031-8914(36)80009-3.

[3] J. Kondo, "Resistance minimum in dilute magnetic alloys," en, *Progress of Theoretical Physics*, vol. 32, no. 1, pp. 37–49, Jul. 1964, ISSN: 0033-068X, 1347-4081. DOI: 10.1143/PTP.32.37.

[4] P. W. Anderson, "A poor man's derivation of scaling laws for the kondo problem," *Journal of Physics C: Solid State Physics*, vol. 3, no. 12, pp. 2436–2441, Dec. 1970, ISSN: 0022-3719. DOI: 10.1088/0022-3719/3/12/008.

[5] K. G. Wilson, "The renormalization group: Critical phenomena and the kondo problem," en, *Reviews of Modern Physics*, vol. 47, no. 4, pp. 773–840, Oct. 1975, ISSN: 0034-6861. DOI: 10.1103/RevModPhys.47.773.

[6] R. Bulla, T. A. Costi, and T. Pruschke, "Numerical renormalization group method for quantum impurity systems," en, *Reviews of Modern Physics*, vol. 80, no. 2, pp. 395–450, Apr. 2008, ISSN: 0034-6861, 1539-0756. DOI: 10.1103/revmodphys.80.395.

[7] A. C. Hewson, *The Kondo problem to heavy fermions* (Cambridge studies in magnetism), eng. Cambridge: Cambridge university press, 1993, ISBN: 978-0-521-36382-2.

[8] H. Krishna-murthy, J. Wilkins, and K. Wilson, "Renormalization-group approach to the anderson model of dilute magnetic alloys. i. static properties for the symmetric case," en, *Physical Review B*, vol. 21, no. 3, pp. 1003–1043, Feb. 1980, ISSN: 0163-1829. DOI: 10.1103/PhysRevB.21.1003.

[9] *Many-body physics: from Kondo to Hubbard: lecture notes of the Autumn School on Correlated Electrons 2015: at Forschungszentrum Jülich, 21-25 September 2015* (Schriften des Forschungszentrums Jülich. Reihe Modeling and Simulation), eng. Jülich: Forschungszentrum Jülich, 2015, ISBN: 978-3-95806-074-6.

[10] P. Nozières and A. Blandin, "Kondo effect in real metals," *Journal de Physique*, vol. 41, no. 3, pp. 193–211, 1980, ISSN: 0302-0738. DOI: 10.1051/jphys:01980004103019300.

[11] P. Schlottmann and P. Sacramento, "Multichannel kondo problem and some applications," en, *Advances in Physics*, vol. 42, no. 6, pp. 641–682, Dec. 1993, ISSN: 0001-8732, 1460-6976. DOI: 10.1080/00018739300101534.